www.sciencetranslationalmedicine.org/cgi/content/full/6/240/240ra75/DC1

Supplementary Materials for

Alkylphosphocholine Analogs for Broad-Spectrum Cancer Imaging and Therapy

Jamey P. Weichert,* Paul A. Clark, Irawati K. Kandela, Abram M. Vaccaro, William Clarke, Marc A. Longino, Anatoly N. Pinchuk, Mohammed Farhoud, Kyle I. Swanson, John M. Floberg, Joseph Grudzinski, Benjamin Titz, Anne M. Traynor, Hong-En Chen, Lance T. Hall, Christopher J. Pazoles, Perry J. Pickhardt, John S. Kuo*

*Corresponding author. E-mail: jweichert@uwhealth.org (J.P.W.); j.kuo@neurosurgery.wisc.edu (J.S.K.)

Published 11 June 2014, *Sci. Transl. Med.* **6**, 240ra75 (2014)
DOI: 10.1126/scitranslmed.3007646

This PDF file includes:

Other Supplementary Material for this manuscript includes the following:
(available at www.sciencetranslationalmedicine.org/cgi/content/full/6/240/240ra75/DC1)

SUPPLEMENTARY MATERIALS

Supplementary Methods

Synthesis of CLR1501

The synthesis of CLR1501 (18-[p-(4,4-difluoro-4-bora-3a,4a-diaza-s-indacene-8-yl)-phenyl]-octadecyl phosphocholine) (fig. S10A) was performed using Liebeskind-Srogl cross-coupling reaction (*38*) of 18-[*p*-(dihydroxyboryl)-phenyl]-octadecyl phosphocholine [**2**] with 8-thiomethyl-BODIPY [**1**] according to the published procedure (*39*). 8-Thiomethyl-4,4-difluoro-4-bora-3a,4a-diaza-s-indacene [**1**] as well as compound [**2**] were synthesized as described previously (*40*).

^{1}H NMR (500 MHz, $CDCl_3$ - CD_3OD 1:1): δ 7.93 (s, 2H), 7.52 (dt, J_1 = 8.3 Hz, J_2 = 1.8 Hz, 2H), 7.38 (dt, J_1 = 8.3 Hz, J_2 = 1.8 Hz, 2H), 7.02 (d, J = 4.1 Hz, 2H), 6.595 (dd, J_1 = 4.1 Hz, J_2 = 1.7 Hz, 2H), 4.23 (br m, 2H), 3.87 (q, J = 6.6 Hz, 2H), 3.60 (m, 2H), 3.22 (s, 9H), 2.75 (t, J = 7.6 Hz, 2H), 1.71 (quintet, J = 7.4 Hz, 2H), 1.64 (quintet, J = 7.1 Hz, 2H), 1.44 – 1.24 (m, 28H). ^{19}F NMR (376.2 MHz, $CDCl_3$ - CD_3OD 1:1): δ -145.8 (q, J = 28 Hz). ESI ultra high-res QTOF MS (*m/z*) calculated for $C_{38}H_{60}BF_2N_3O_4P$ ($[M+H]^+$) 701.441339, found 701.44041; calculated for $C_{38}H_{59}BF_2N_3O_4PNa$ ($[M+Na]^+$) 723.423283, found 723.42221.

Synthesis of CLR1502

CLR1502 was synthesized (fig. S10B) by the Suzuki cross-coupling reaction of 18-[*p*-(dihydroxyboryl)-phenyl]-octadecyl phosphocholine [**2**] with commercially available fluorescent dye IR-775 in the presence of a catalyst, Pd-PEPPSI-IPr. CLR1403 (1.322 g, 2.38 mmol), dye IR-775 chloride (1.856 g, 3.57 mmol), potassium carbonate (987 mg, 7.14 mmol) and Pd-PEPPSI-IPr (80 mg, 0.12 mmol) were placed in a 100 ml round-bottom flask and kept under high vacuum for 30 min. Degassed methanol was added via cannula and the reaction mixture was stirred at room temperature for 20 h checked by TLC in 3 systems: silica gel ($CHCl_3$-MeOH-H_2O 10:6.5:1.5) and $CHCl_3$-MeOH-conc NH_4OH 65:25:4) and also amino-silica gel ($CHCl_3$-MeOH-H_2O 65:25:1). Chloroform (10-15 ml) was added and the mixture was filtered using a glass fritted funnel to remove inorganic salts. Filtrate was loaded on silica gel column. The column was eluted first with stepwise gradient of $CHCl_3$ - MeOH (90:10, 80:20, 50:50) - 500 ml each and finally with $CHCl_3$ – MeOH – H_2O (65:25:4) – 1880 ml, then with $CHCl_3$ – MeOH – H_2O (65:35:5) – 380 ml and finally with $CHCl_3$-MeOH-conc NH_4OH (65:25:4). Fractions containing CLR1502 were combined and analyzed by TLC and NMR. The purest fraction weighed 889 mg (38%).

^{1}H NMR (500 MHz, $CDCl_3$ - CD_3OD 1:1): δ 7.43 (dm, J = 8 Hz, 2H), 7.37 (dt, J1 = 7.9 Hz, J2 = 1.3 Hz, 2H), 7.31 (d, J = 14.1 Hz), 7.25 (dd, J1 = 7.5 Hz, J2 = 0.9 Hz, 2H), 7.19 (dt, J1 = 7.3 Hz, J2 = 0.9 Hz, 2H), 7.16-7.14 (m, 4H), 6.06 (d, J = 13.9 Hz, 2H), 4.25 (m, 2H), 3.86 (q, J = 6.6, 2H), 3.62 (m, 2H), 3.56 (s, 6H), 3.24 (s, 9H), 2.82 (t, J = 7.3 Hz, 2H), 2.71 (t, J = 6.2 Hz, 2H), 2.08 (m, 2H), 1.76 (m, 2H), 1.62 (quintet, = 7.1 Hz, 2H), 1.48 – 1.24 (m, 28H), 1.21 (s, 12H). ^{31}P NMR (202.3 MHz, $CDCl_3$ - CD_3OD 1:1): 1.07 (s).

ESI ultra high-res QTOF MS (m/z) calcd for $C_{61}H_{89}N_3O_4P$ ([M-Cl]+) 958.65852, found 958.65399; 479.32869 ([M-Cl + H]2+/2).

Normal cell and cancer cell co-culture

The PC-3 (human prostate carcinoma) cell line and normal human fibroblasts were plated overnight on microslide VI (Ibidi). The next day, the cells were treated with 5 µM of CLR1501 for 24 hours. The cells were counter stained with the nuclear stain, Hoechst 33342 (Invitrogen). The cells were examined using Nikon A1R confocal microscope. The emission signal of CLR1501 was detected using Alexa Fluor 488 filters. Hoechst 33342 was detected using Hoechst filters (ex/em 350/461 nm).

In vitro uptake and retention of ^{125}I-CLR1404

In vitro uptake/retention quantification of ^{125}I-CLR1404 was performed in human cancer and normal cells as follows. Briefly, cells were plated at $5.0x10^4$ cells per well in six well plates using the appropriate serum containing media, and allowed to adhere overnight. The next day, each well was washed with 2 ml of serum-free media after which FBS-containing media with 1.5 µCi of ^{125}I-CLR1404 was added to each well (2 ml media/drug mixture per well, in triplicate). Cells were then incubated at 37^{o}C and 5% CO2 in air for the indicated time period. After various times of incubation, for each replicate, the media was removed and wells were washed twice with 1ml of 1× PBS containing 0.1% BSA. The cells were then trypsinized, scraped, mixed and divided evenly into two 0.5 ml aliquots. For sample measurement, radioactivity in 10 µl from each sample was measured with a gamma counter for ^{125}I using a commercial ^{125}I standard and a standard curve using serial diluted ^{125}I-CLR1404. The other cell fraction aliquot was centrifuged for 30 seconds at 14,000 x g, and the cell pellet was dissolved in 100 µl of 1× PBS. The DNA content was determined by absorbance at 260nm and absorbance at 320 nm was used for turbidity correction. Total cell number was determined by comparison to a standard curve of 260 nm absorbance values of known cell numbers. From these data, radioactivity per cell was calculated as pCi per cell.

Live cell flow cytometry

Cultured human GSCs or other cells were treated for 24 hrs with 10 µM CLR1501 or vehicle (1% ethanol) controls. Approximately 10^6 cells were enzymatically dissociated from spheres and resuspended in flow cytometry buffer (PBS+1% goat serum). Pre-conjugated AC/CD133 with allophycocyanin (APC; Miltenyi Biotech 130-090-826) was added to the suspension (1:11) to label GSCs and incubated for 1 hr on ice. It is important to note that the anti-CD133 antibody used in this study specifically targets the stem cell-specific glycosylated form of AC/CD133, and that other glycosylated or non-glycosylated forms of CD133 protein are likely expressed in the AC/CD133$^-$ population (*41*).

Cells were washed multiple times and analyzed using flow cytometry (FACScalibur, Becton Dickinson). The flow cytometer was corrected for background fluorescence (no antibody control) and spectral bleed-through (compensation with single labeled cells). Data were collected on 10,000 cells by gating for CLR1501 (490/515) and

AC/CD133-APC (650/660), and analyzed using WinMDI freeware (http://facs.scripps.edu/software.html). Live cells were gated using forward (FSC) and side (SSC) scatter. Proper gating was established to quantify positive vs. negative fluorescent cells by comparing to isotype controls. Intensity is represented by relative fluorescent units (RFU) or the geometric mean of resultant histograms (fig. S4). For in vivo studies, tumor xenografts were microscopically dissected from mouse brains with special care to avoid normal brain parenchyma. Tumor pieces were enzymatically dissociated using Accutase for 15 min followed by mechanical trituration with P200 pipette. The resultant slurry was passed through a 40-µm cell strainer before the AC/CD133 staining procedure.

GSC orthotopic xenograft model

All described animal studies were performed according to animal protocols approved by Institutional Animal Care and Use Committee. GSC-derived orthotopic xenografts were initiated as previously described (*11*, *24*). Cells were stereotactically injected into the right striatum of anesthetized non-obese diabetic severe combined immunodeficient (NOD-SCID) mice at the following coordinates referenced from bregma: 0 mm antero-posterior, +2.5 mm medio-lateral, and -3.5 mm dorso-ventral. At either 3 months or onset of neurological symptoms, in vivo tumor formation was verified using magnetic resonance imaging [mice are anesthetized with isofluorane and contrast enhanced 10 mmol/kg of intra-peritoneal gadodiamide (Omniscan)], placed into a 4.7-T horizontal bore small animal MRI scanner (Varian) and T1- and T2-weighted images obtained. After MRI showed tumor xenograft growth or when neurological symptoms were observed, injected NOD-SCID mice were euthanized by perfusion fixation with 4% paraformaldehyde (PFA). Brains were then excised and embedded in paraffin for general histology or processed for frozen sectioning. For CLR1404 studies, after overnight fixation in 4% paraformaldehyde, brains were embedded in OCT compound and frozen for cryostat sectioning at 5-20 µm. This different processing approach was used because CLR1404 and analogs are soluble in the ethanolic dehydration steps required during paraffin processing.

Lipid raft staining and disruption

The cell line A549 (human non-small lung adenocarcinoma) was plated overnight on microslide VI (Ibidi) in serum containing media (F-12 media supplemented with 10% fetal bovine serum). The next day, the cells were incubated with 5 µM CLR1501 at 37ºC for 30 minutes. The cells were then washed with phosphate buffered saline and incubated with Cholera Toxin β-subunit (CTB) and anti-CTB for 10 and 15 minutes, respectively at 4ºC to label ganglioside GM1. The cells were fixed with 4% formaldehyde at 4ºC for 15 minutes and washed with phosphate buffered saline. Cholesterol was stained using 0.5 mg/ml filipin III for 30 minutes at 37ºC.

PC-3 cells were pretreated with either 2 µg/ml filipin III or vehicle for 15 min, then washed and incubated with 2 µCi of ^{125}I-CLR1404 for 1 h. The media was removed and the cells were washed with phosphate buffered saline containing 0.1% bovine serum

albumin, trypsinized, then split into two samples for determination of cell number by DNA content (A_{280} compared to a cell line specific standard curve) and counts per minute using a Gamma Counter (Perkin Elmer).

Immunohistochemistry

Primary and secondary antibodies were purchased commercially: human-specific nestin (MAB5326, Millipore), Olig2 (sc-48817, Santa Cruz Biotechnology), and CD15/SSEA-1 (555400, BD Pharmingen); and goat anti-IgG secondary antibodies Alexa Fluor 488 and 568 (Invitrogen). Frozen GSC xenograft samples were first rehydrated to water. Samples were then blocked in 10% goat serum for 1 hour prior to overnight incubation in primary antibody. After thorough rinsing with PBS, species-specific secondary antibody was applied for 1 h. Last, nuclear counterstaining with DAPI or TO-PRO-3 was performed prior to mounting in aqueous mounting medium (Prolong Gold Antifade reagent, Invitrogen).

MicroPET tumor imaging with ^{124}I-CLR1404 and ^{18}F-FDG in the presence of inflammation

Prostate tumor cells (1×10^6 PC3 cells in 100 µl PBS) were implanted into the thigh muscle on one leg and injected directly into the tibia (via knee joint) of the contralateral leg to simulate a bone metastasis in nude mice (n = 6). A carageenan-induced granuloma (600 µl air pouch injected with 200 µl 1% carageenan in sterile water) was created subcutaneously between the scapulae in each mouse. Five days after induction of the granuloma, ^{18}F-FDG (200 µCi, 0.1 ml) was injected intravenously via lateral tail vein into anesthetized (isoflurane) mice. One hour later, while under anesthesia, animals underwent whole body microPET scanning (Siemens Inveon, 40 million counts collected). Following scanning, animals were injected intravenously with ^{124}I-CLR1404 (0.2 ml, 85-110 µCi). Comparative microPET scans were performed 24 h later under identical conditions. By this time the ^{18}F signal had returned to background levels. Granulomas to tumor ratios were calculated by ROI analysis.

SUPPLEMENTARY FIGURES

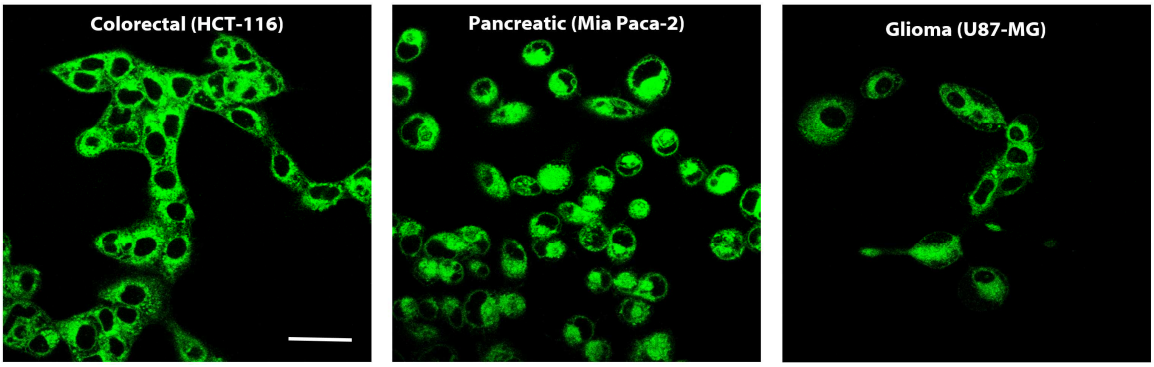

Fig. S1. **Preferential cancer cell uptake of CLR1501**. Fluorescence confocal microscopy illustrates that the fluorescent CLR1404 analogue, CLR1501, is selectively retained in three additional cancer types at 24 hours post-treatment. The other cell lines are shown in Fig. 2A. Scale bar, 10 µm.

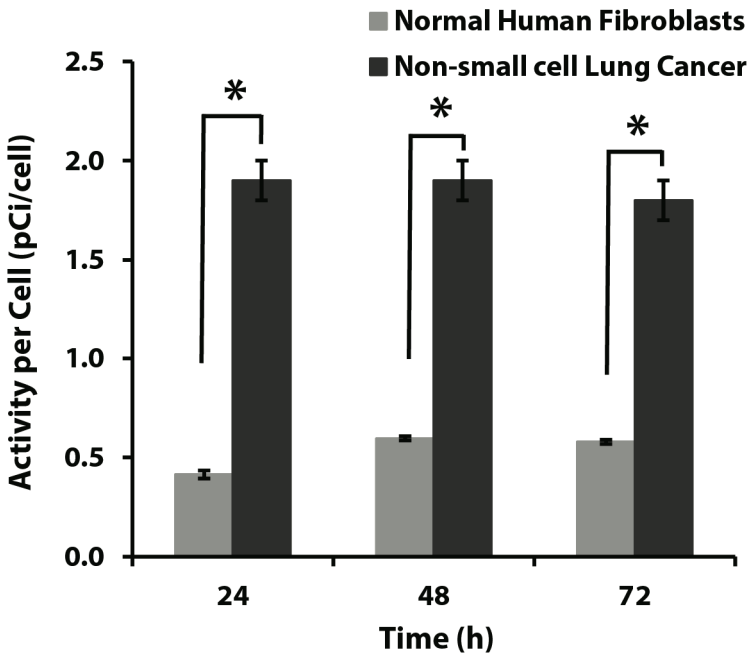

Fig. S2. Preferential ^{125}I-CLR1404 uptake and retention in cancer cells in vitro. Uptake and retention of ^{125}I-CLR1404 in the A549 (human NSCLC) cell line relative to normal primary human fibroblasts at various time points. Data are means ± S.E.M. (n = 3 independent experiments with 3 biological replicates each). *P<0.001, ANOVA with post-hoc Tukey test.

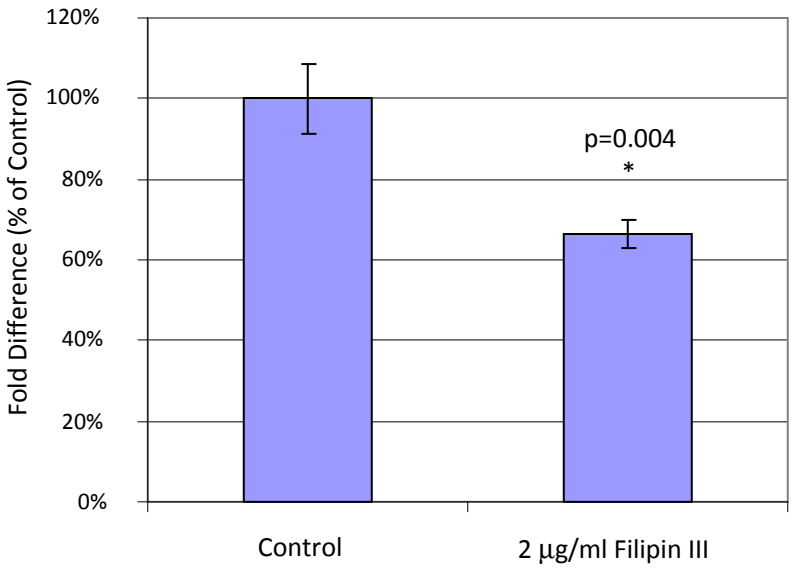

Fig. S3. Uptake and retention of ^{125}I-CLR1404 after lipid raft disruption in prostate carcinoma cells. PC-3 cells were pretreated with either filipin III or vehicle, then incubated with ^{125}I-CLR1404 for 1 h. DNA content (compared to a cell line–specific standard curve) and counts per minute were calculated. Data are average ± SEM (*n* = 6). *P*-value determined by t-test.

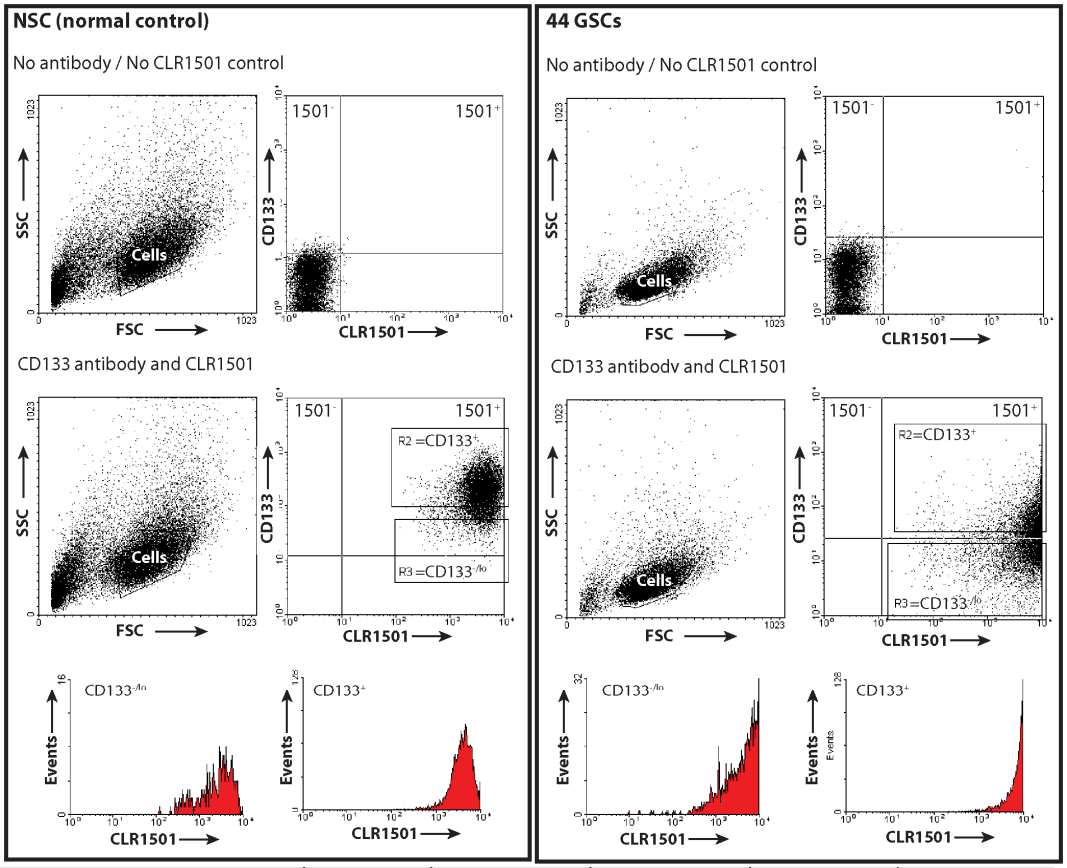

	NSC	12.1 GSC	22 GSC	33 GSC	44 GSC	99 GSC
Gmean [RFU]	3570 ± 169	7380 ± 1010	7410 ± 301	6160 ± 487	5780 ± 756	7860 ± 193
CD133^{+} [RFU]	3740 ± 53.3	8740 ± 560	7530 ± 352	5860 ± 237	7350 ± 895	8050 ± 205
CD133^{-} [RFU]	2290 ± 1250	5380 ± 1130	4030 ± 303	6940 ± 659	4010 ± 486	6190 ± 593
p-value CD133^{+} vs CD133^{-}	0.12	0.02	0.0037	0.047	0.0088	0.016
p-value GSC vs NSC	N/A	0.00046	0.00027	0.00011	0.0022	3.90e-06

Figure S4: **Flow cytometry analysis of CLR1501 GSC labeling.** After overnight labeling with CLR1501, GSC and NSC spheres were dissociated to single cells, immunolabeled with CD133, and analyzed by flow cytometry. Cellular fraction was first gated by SSC/FSC plots. Baseline values were determined through use of no CLR1501 / no primary antibody controls for each cell line, and used to construct quadrants for positive and negative labeling of cells. With the CD133 antibody, regions were chosen to represent CD133^{+} and CD133$^{-/lo}$ populations of GSCs and NSCs. These regions were analyzed for average fluorescent intensity (geometric mean), which is presented in the table from triplicate flow cytometry runs. Data in table are means ± SD of 3 independent experiments. *P*-values determined by Student's t-test.

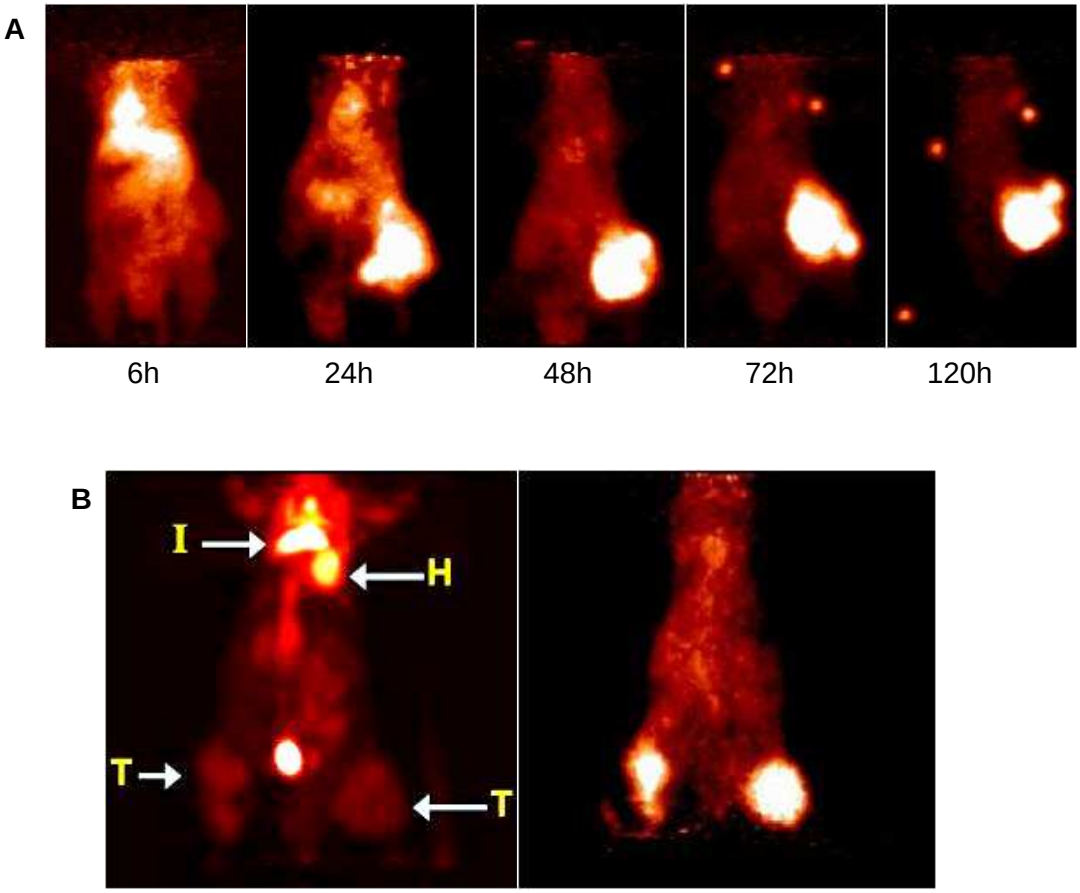

Figure S5. **In vivo time course of biodistribution and tumor uptake of ^{124}I-CLR1404 and ^{18}F-FDG in a prostate tumor model.** (**A**) A SCID mouse bearing a subcutaneous flank PC-3 (human prostate carcinoma) xenograft. Spatial fiducial markers in the 72 h and 120 h panels were used for image fusion. (**B**) MicroPET projection view images of a mouse with human PC3 tumors (T) in the right flank and pseudo metastasis in the left tibia (T), a Carageenan-induced inflammatory lesion (I) located between the scapulae, and heart (H). Left image was acquired 1 h after administration of ^{18}F-FDG. Right image was obtained 24 h after administering ^{124}I-CLR1404 to the same mouse, 24 h after the FDG scan.

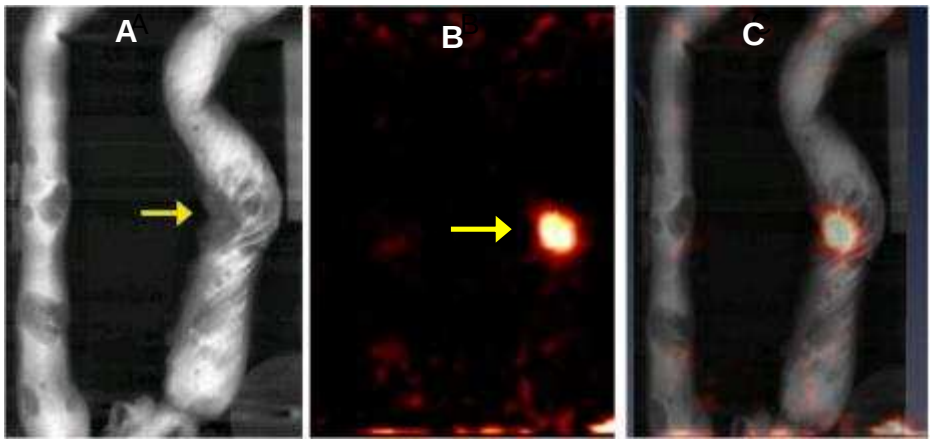

Fig. S6. Dual modality PET/CT virtual colonoscopy in rodents. (**A** to **C**) An excised Pirc rat colon filled with 2% barium positive contrast and imaged with 2D-microCT projection (A) and ^{124}I-NM404 microPET (B). The fusion of (A and B) is shown in (C). The only tumor (arrow) that was positive on ^{124}I-CLR404 microPET was the only malignant one of 20 total colon lesions (movie S2).

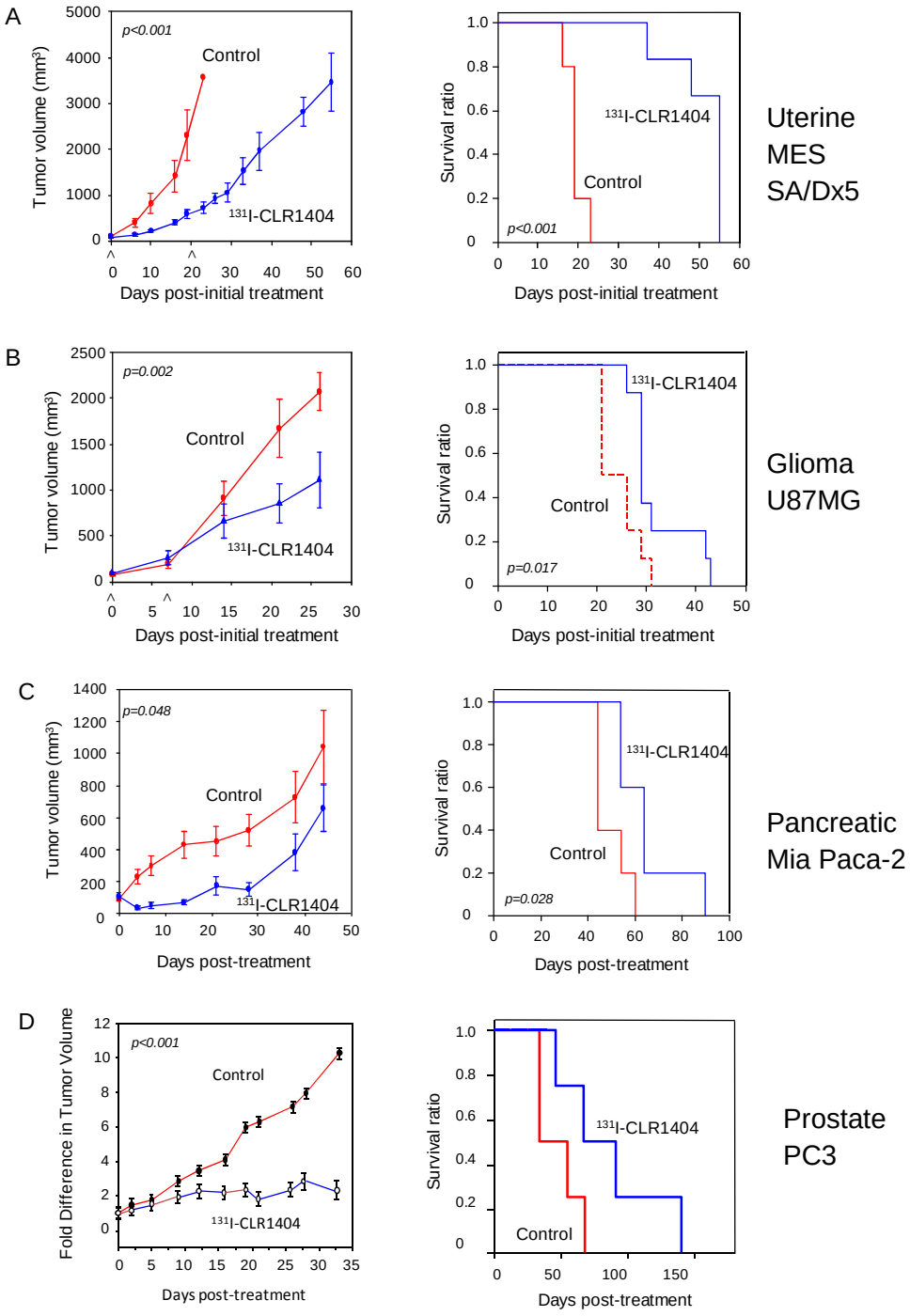

Fig. S7. **Tumor growth and animal survival after ^{131}I-CLR1404 therapy.** Radiotherapy in human tumor xenografts was tested. ^{131}I-CLR1404 dosing was as follows: (**A**) uterine, day 0 130 µCi, day 20 145 µCi (*n* = 6); (**B**) glioma, days 0 and 7, 100 µCi each (*n* = 8); (**C**) pancreatic, day 0 125 µCi (*n* = 5); (**D**) prostate, day 7, 100 µCi (*n* = 6). Control animals (*n* = 6) were administered an approximate mass-equivalent of non-radioactive CLR1404 dose on Day 0. Tumor volumes are means ± SEM. Survival curves were constructed by Kaplan-Meier method and analyzed via Log-rank test for significance. *P*-values determined by one-way repeated measurement ANOVA.

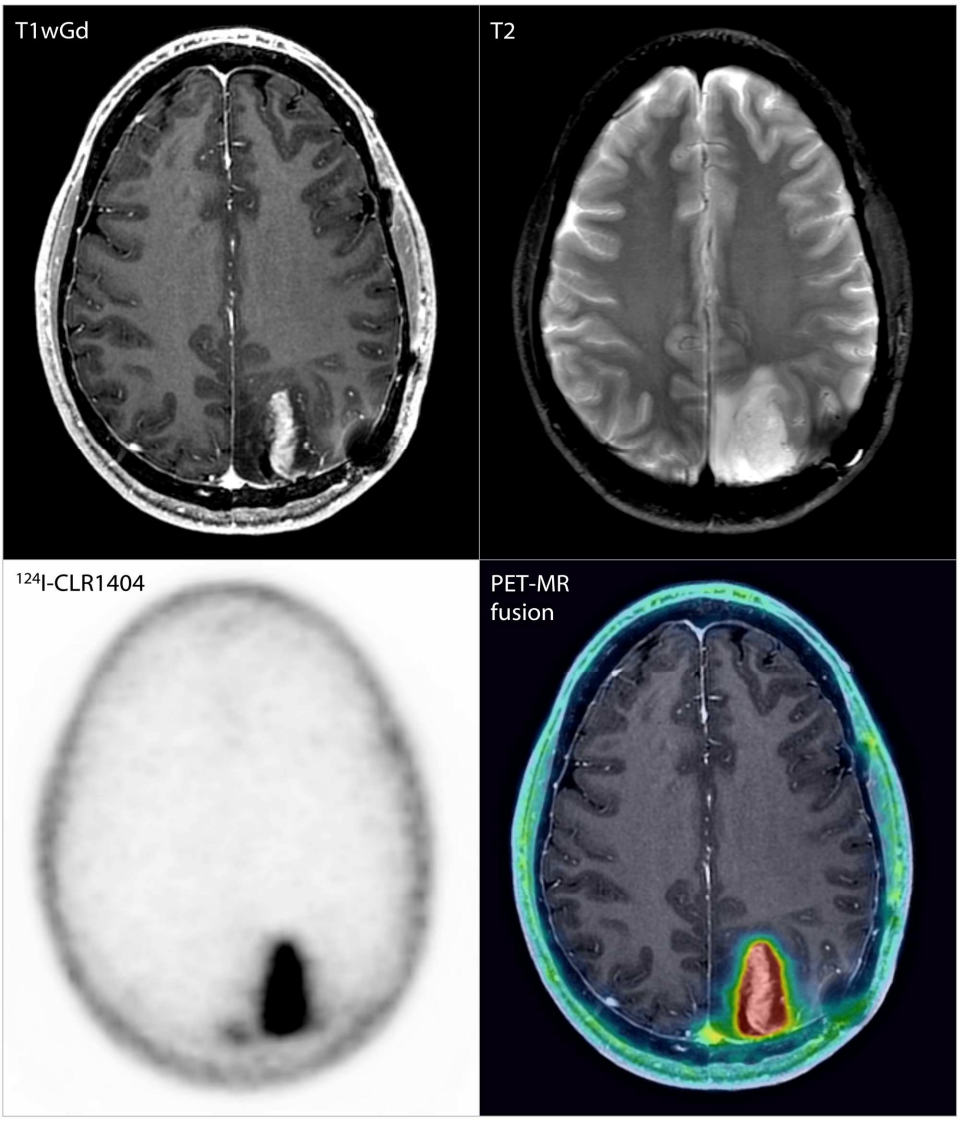

Fig. S8. Recurrent World Health Organization grade III astrocytoma. Left parietal astrocytoma was resected 2 years before this axial T1-contrast MR and PET imaging that show likely recurrence in a patient with grade II/III glioma.

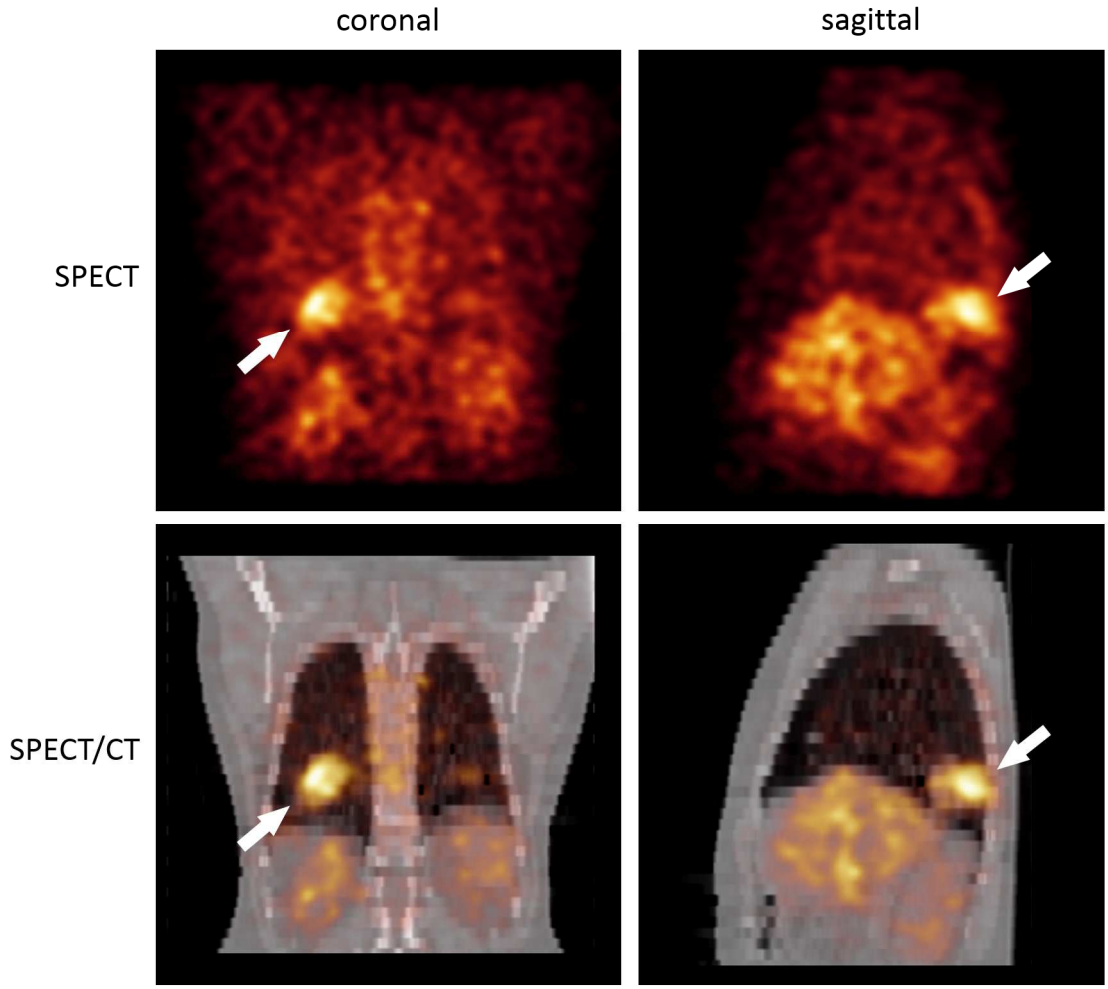

Fig. S9. ^{131}I-CLR1404 SPECT/CT imaging of metastatic colorectal cancer. Coronal and sagittal SPECT images and corresponding fused SPECT/CT images of a recurrent colorectal cancer patient with lung and liver metastases (arrow). Images were obtained 21 days after injection of ^{131}I-CLR1404.

A

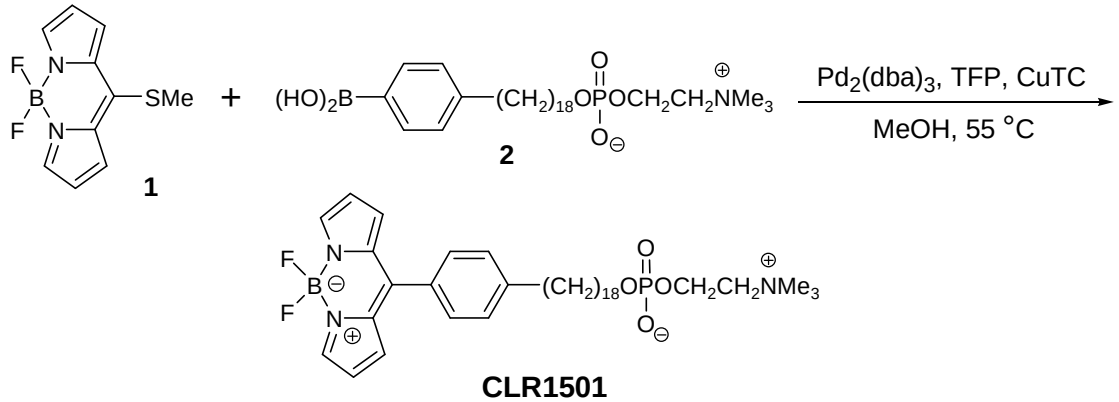

$Pd_2(dba)_3$ = tris-(dibenzylideneacetone) dipalladium (0)

TFP = tri-(2-furyl) phosphine =

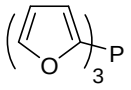

CuTC = copper (I) thiophene-2-carboxylate =

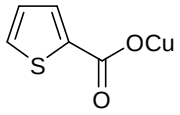

B

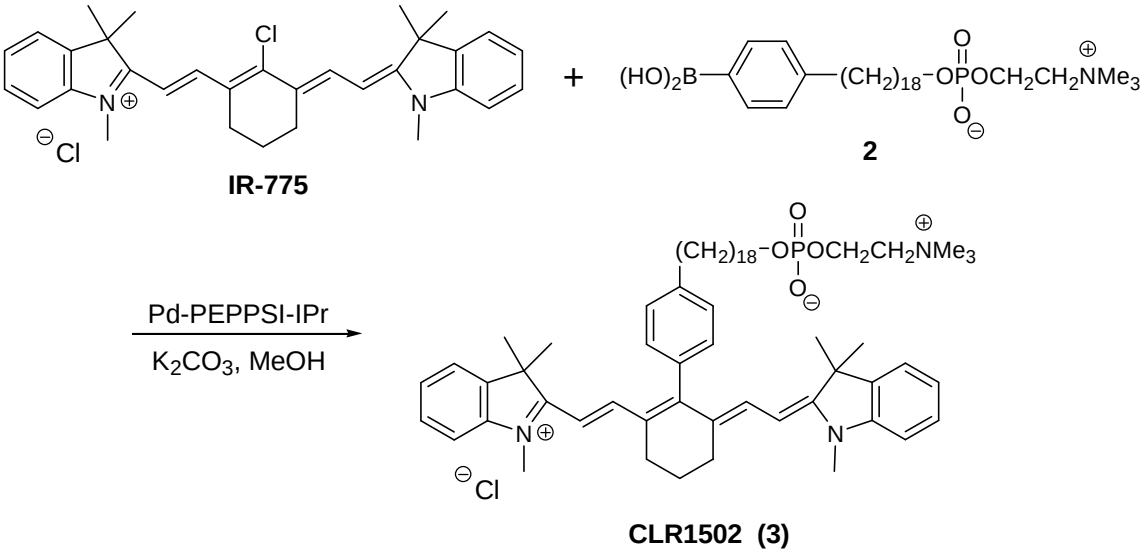

Figure S10. Synthesis of optical APC analogs. (**A**) Fluorescent analog CLR1501. (**B**) NIR analog CLR1502. [**1**] 8-thiomethyl-BODIPY; [**2**] 18-[*p*-(dihydroxyboryl)-phenyl]-octadecyl phosphocholine.

Supplementary Tables

Table S1: ^{124}I-CLR1404 uptake in tumor xenografts. Tumor uptake was considered positive if tumor to muscle ratio was > 3. Tumor:muscle ratio $\leq$ 2 was considered negative.

Tumor model		Species	Category	Tumor uptake[1]
1	Prostate PC-3	SCID mouse	Adenocarcinoma	Yes
2	Lung A-549 (NSCLC)	SCID mouse	Adenocarcinoma	Yes
3	Lung NCI H-69 (Oat Cell)	SCID mouse	Small cell carcinoma	Yes
4	Adrenal H-295	SCID mouse	Adenocarcinoma	Yes
5	Adrenal RL-251	SCID mouse	Adenocarcinoma	Yes
6	Colon-51	SCID mouse	Adenocarcinoma	Yes
7	Colon LS180	SCID mouse	Adenocarcinoma	Yes
8	Colon DLD1	SCID mouse	Adenocarcinoma	Yes
9	Colon HT-29	SCID mouse	Adenocarcinoma	Yes
10	Colon LS-180	Nude mouse	Adenocarcinoma	Yes
11	Glioblastoma U87	Nude mouse and NOD-SCID (orthotopic)	Glioma	Yes
12	Melanoma A-375	Nude mouse	Adenocarcinoma	Yes
13	Multiple myeloma MM.1S	Nude mouse	Myeloma	Yes
14	Neuroblastoma SK-N-AS	Nude mouse	Neuroblastoma	Yes
15	Neuroblastoma NB1691	Nude mouse	Neuroblastoma	Yes
16	Neuroblastoma CHLA-20	Nude mouse	Neuroblastoma	Yes
17	Neuroblastoma Lan5	Nude mouse	Neuroblastoma	Yes
18	Ovarian HTB-77	Nude mouse	Adenocarcinoma	Yes
19	Ovarian Ovcar-3	Nude mouse	Adenocarcinoma	Yes
20	Pancreatic BXPC3	Nude mouse	Adenocarcinoma	Yes
21	Pancreatic Mia Paca-2	Nude mouse	Carcinoma	Yes
22	Pancreatic Capan-1	Nude mouse	Adenocarcinoma	Yes
23	Renal cell Caki-2	Nude mouse (orthotopic)	Clear cell carcinoma	Yes
24	Renal cell ACHN	Nude mouse (orthotopic)	Adenocarcinoma	Yes
25	Sarcoma (Meth-A)	Nude mouse	Fibrosarcoma	Yes
26	Head and neck SCC1	Nude mouse	Squamous cell carcinoma	Yes
27	Head and neck SCC6	Nude mouse	Squamous cell carcinoma	Yes
28	Prostate LNCap	Mouse	Adenocarcinoma	Yes
29	Prostate LuCap	Mouse	Adenocarcinoma	Yes
30	Breast MCF-7	Rat	Adenocarcinoma	Yes

31	Triple negative breast MDA-MB231	Nude mouse	Adenocarcinoma	Yes
32	Uterine MES SA/Dx5	Nude mouse	Sarcoma	Yes
33	Glioblastoma 22 GSC	NOD-SCID mouse (orthotopic)	Glioma	Yes
34	Glioblastoma 105 GSC	NOD-SCID mouse (orthotopic)	Glioma	Yes
35	Breast 4T1	Endogenous mouse (orthotopic)	Adenocarcinoma	Yes
36	Bladder SV40	Mouse (orthotopic)	Adenocarcinoma	Yes
37	Prostate MatLyLu	Rat	Adenocarcinoma	Yes
38	Walker256	Rat	Carcinosarcoma	Yes
39	TRAMP prostate	Endogenous mouse	Adenocarcinoma	Yes
40	Colon CT26	SCID mouse	Adenocarcinoma	Yes
41	Colon Pirc	Autochthonous Pirc rat	Adenocarcinoma	Yes
42	Min mouse intestinal	Endogenous mouse	Adenocarcinoma	Yes
43	Melanoma	Mouse	Adenocarcinoma	Yes
44	Mammary SCC	$Apc^{Min/+}$ mouse	Squamous cell carcinoma	Yes
45	Mammary AC	$Apc^{Min/+}$ mouse	Adenocarcinoma	Yes
46	Hepatocellular carcinoma	Endogenous mouse	Adenocarcinoma	Yes
47	Glioma L9	Rat xenograft	Glioma	Yes
48	Glioma C6	Rat xenograft	Glioma	Yes
49	Glioma CNS1	Rat xenograft	Glioma	Yes
50	Glioma RG2	Rat xenograft	Glioma	Yes
51	Retinoblastoma	Endogenous mouse	Blastoma	Yes
52	Pancreatic c-myc	Endogenous mouse	Adenocarcinoma	Yes
53	Pancreatic Kras	Endogenous mouse	Adenocarcinoma	Yes
54	Cervical-HPV	Endogenous mouse	Adenocarcinoma	Yes
55	Esophageal	Endogenous Mouse	Adenocarcinoma	Yes
1	Intestinal polyp	Endogenous mouse	Adenoma (benign)	No
2	Mammary alveolar hyperplasia	Endogenous mouse	Hyperplasia (benign)	No
3	Hepatoma Hep-3B	Nude mouse	Carcinoma	No
4	Hepatoma Hep-G2	Nude mouse	Carcinoma	No
5	Pirc rat colon adenoma	Pirc rat	Adenoma	No

Table S2. Patient information.

Figure	Diagnosis	CLR1404	Dose (mCi)	Imaging modality
7A	Non-small cell lung cancer (NSCLC)	^{124}I	5	PET/CT
7B-D	Grade IV glioma	^{124}I	5	PET/CT
S8	Grade II/III glioma	^{124}I	5	PET/CT
S9	Colorectal cancer	^{131}I	25	SPECT

SUPPLEMENTARY VIDEOS

Movie S1. Cellular uptake of CLR1501 in prostate cancer cells. PC3 (human prostate adenocarcinoma), was stained with MitoTracker Red CMXRos dye and blue-fluorescent Hoechst 33342 dye for mitochondrial and nuclear imaging, respectively. Image acquisition started upon adding 5 μM CLR1501 *in vitro* and continued for 1 hour.

Movie S2. Dual modality PET/CT virtual colonoscopy in the Pirc rat model. Endoluminal fly through of rat colon showing premalignant adenomas (yellow masses) and one malignant adenocarcinoma (red mass).